EXPERIMENTAL SETUP OF A PULSED MPD THRUSTER AT IRS

A. Nawaz, M. Auweter-Kurtz, G. Herdrich, H. Kurtz
Universität Stuttgart – Institut für Raumfahrtsysteme, Stuttgart, Germany

An instationary pulsed magnetoplasmadynamic thruster (I-MPD) called SIMP-LEX (**S**tuttgart **In**stationary **M**agneto**p**lasmadynamic Thruster for **L**unar **Ex**ploration) is being devised as primary propulsion system on an all electrical lunar mission. For this purpose a variation of the thruster parameters propellants type, electrode length and distance between electrodes was carried out using a modular setup of the I-MPD. Between pure Polytetrafluorethylen (PTFE) and PTFE to which a small amount of MoS2 was added, pure PTFE yielded better results as propellant. A smaller distance between the electrodes leads to higher exhaust velocities but lower mean thrust levels as well as efficiencies. Further, a description of the instruments and facilities used is given. Higher exhaust velocities were given priority over thrust level and efficiency due to the nature of this lunar mission

Introduction

At the *Institut für Raumfahrtsysteme* (IRS), University of Stuttgart, Germany, an instationary pulsed magnetoplasmadynamic thruster (I-MPD) is being devised. These thrusters are also referred to as pulsed plasma thrusters (PPT).

The development of these thrusters was initiated when the IRS decided in 2002 to successively launch four satellite missions from 2006/2007 onwards: 1- FlyingLaptop, a micro satellite for earth observation [1], 2- CERMIT, a re-entry mission [2], 3- a mission to test the electric thrusters developed and 4- BW-1, an all-electrical lunar mission [3]. The I-MPD thruster described herein is called SIMP-LEX (Stuttgart Instationary Magnetoplasmadynamic Thruster for Lunar Exploration) and is being designed for the last mission, BW-1.

The lunar mission is scheduled for launch by the end of this decade. The cube of 1 m^3 will be propelled by an arcjet also developed at IRS [4] and a cluster of I-MPDs. It is intended to use the arcjet during phases requiring higher thrust levels of around 100 mN. However, the prevailing thruster used during the journey is SIMP-LEX. BW-1 will carry several cameras and other instrumentation for the scientific part of the lunar mission.

In principle, a parallel plate I-MPD consists of two parallel electrode plates between which a solid propellant (Polytetrafluorethylen, PTFE) block is placed, see Fig.1. The capacitor is charged externally and discharges across the surface of the PTFE, forming PTFE-plasma once the igniter is fired.

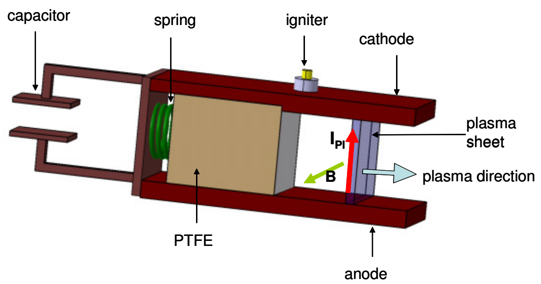

Fig.1 Working Principle of an ablative I-MPD

An electrical circuit with current I_{Pl} and its own magnetic field B is formed. Consequently the thrust forms when the plasma is accelerated outwards along the electrodes according to the Lorentz law.

I-MPDs combine several advantages, specifically regarding small satellites [5]. The most important advantage, particularly for small satellites results from the pulsed energy release. This allows for low average power and the use of broad power ranges without loss of performance. Power is usually one of the tightest constraints on board small satellites.

First rough estimates require SIMP-LEX to perform about 26 million pulses at an average of 1.5 mN providing a Δv of ~5 m/s. In order to reach this ambitious goal, investigations at IRS include characterisation as well as life expectancy of the thruster in up to three different test facilities.

Current Setup of Facility and Equipment

In its final stage the test facility will be comprised of three vacuum chambers. One contains the thrust balance, one for life expectancy tests and one for measuring other parameters e.g. through spectroscopy. Currently, the first chamber is already in use and the life expectancy chamber is being setup. The vacuum chamber used for the tests presented here can be seen in figure 2.

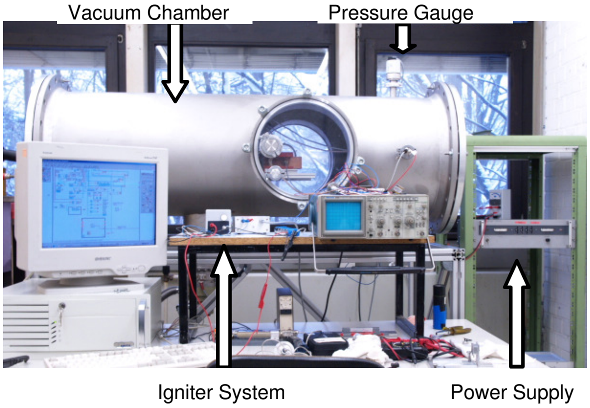

Fig.2 One of Three I-MPD Test Facilities

It is a cylindrical stainless steel chamber with a diameter of 0.5 m and a length of 1.6 m. The pump system, consisting of a rotary vane pump and a turbomolecular pump, reaches pressures of 1.5 x 10^{-5} mbar. The chamber is equipped with a pressure gauge. Power supply for the capacitor and the igniter is provided from outside the chamber.

On the thruster side, the current setup is devised for being highly modular in order to allow changes of parts and geometry. Figure 3 shows the laboratory model SIMP-0 mounted on anodized aluminum channels. These serve as variable support of the thruster design as well as frame for mounting on the thrust balance. The 40 μF, 2000 V cylindrical capacitor can be seen at the back. A detailed view of the electrodes is shown in figure 4.

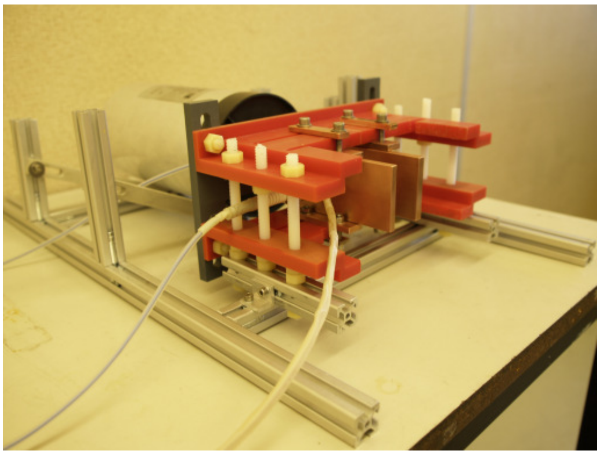

Fig.3 Current Setup of the Modular I-MPD SIMP-0

Two Polyethylen (PE) half-shells keep the copper electrodes in place and parallel to each other. This design makes changes in width, height or length of electrodes easy. The cathode, the left electrode, is threaded to hold the igniter. Several off-the-shelf igniters were tested. The igniter shown in fig.4 is a regular auto-spark plug. However, because of its projected nose side electrode and its exposure to the plasma in the channel, this spark plug was replaced by an auto racing spark plug. Racing spark plugs have a flat surface and are therefore more adequate for this application.

While the PTFE plasma moves outwards along the electrodes, carbon – stemming from the PTFE plasma itself – settles on the inside of the half-shells. Since carbon is an electrically conducting material it was necessary to interrupt the circuit between the copper electrodes via the carbon-sheeted half shells. The cut can be seen in the center between the electrodes in figure 4. Figure 5 shows SIMP-0 in operation.

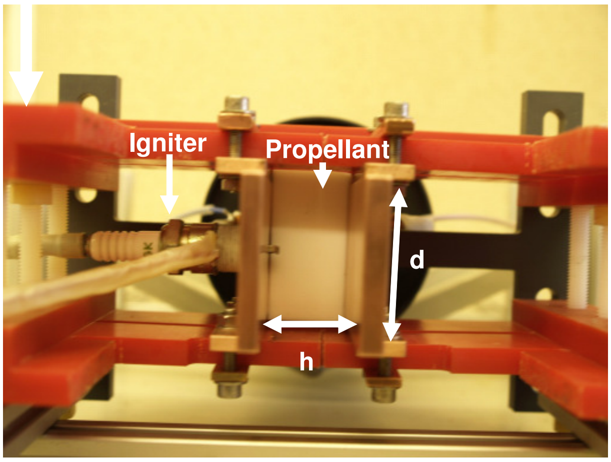

Fig.4 Close-Up of I-MPD Showing Geometry

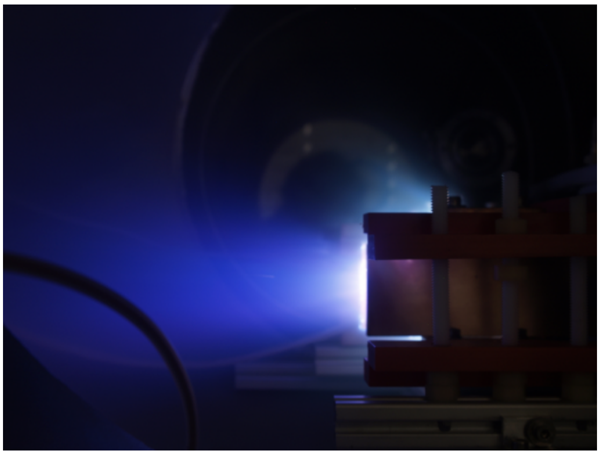

Fig.5 Side View of Simp-0 during Experiment

Variation of geometry, material and parts used is done in order to characterize and optimize the thruster for the mission. The parameters that were investigated here are the distance h between the electrodes, the PTFE type and the length L of the electrodes. Further parameters include the width d of the electrodes, the capacitor type, the electrode material, the propellant shape and others.

The distance h between the electrodes as seen in figure 4 was varied between 19 mm, 29 mm and 39 mm. The PTFE types tested include pure PTFE as well as PTFE to which a small percentage of molybdenum sulfate MoS_2 was added. A possible reduction in energy needed to ablate the metal-containing propellant was hoped to lead to an increase in efficiency. After the optimal configuration was found from these two parameters, the length L was varied from 80 mm through 47 mm in order to optimize circuit behavior.

Measurement System

The measurement system includes all instruments and methods used to record parameters of the thruster during operation. These parameters characterize the thruster's performance.

Apart from the pressure the average mass bit ablated per pulse and the current within the plasma were recorded.

Mass bit

The mass bit was determined by measuring the mass of the PTFE block prior to and after test. A constant value for the ablated mass per pulse was assumed since the pulses were fired under identical conditions. An electronic weight balance with an accuracy of 10 micrograms was used. The accuracy is in the order of magnitude of the mass bit itself. To reduce error, measurements were taken after 150-200 pulses.

Current

The current was measured during pulses using a Pearson Electronics™ current monitor. This monitor consists of a ring-shaped magnetic core around which a coil is wound. This technology makes use of the fact that the magnetic field generated by a current is proportional to the current itself. The output voltage for the used model can range from 0–60 V and corresponds to the current by a factor of 1000. The monitor is mounted between the cathode and the capacitor as seen in figure 7.

The data from the current monitor was read out by a GageSDK™ Compuscope PC card at a rate of 200 MHz.

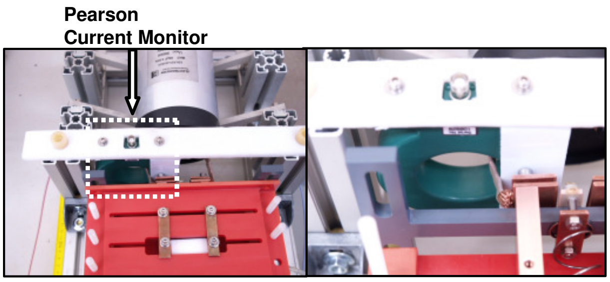

Fig. 7 Integration of the Pearson Current Monitor

Thrust Balance

The thrust balance that is being designed for the I-MPD is a vertical pendulum. It consists of three main parts: the pendulum itself, the support on which the bearing is mounted and a measurement unit, detached from the system placed at the end of the pendulum.

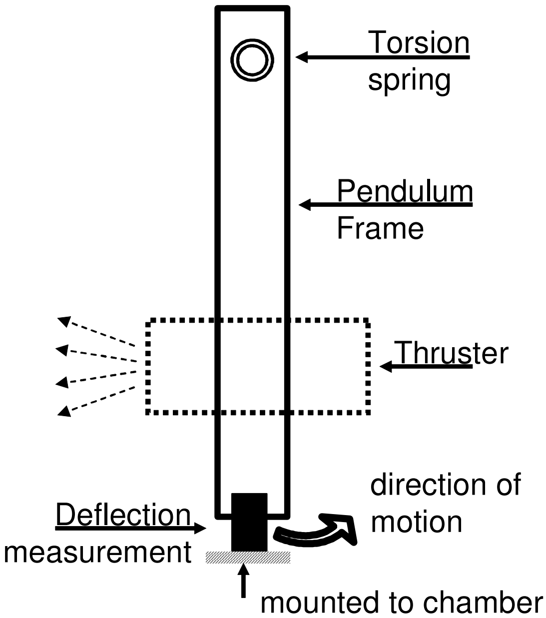

Fig. 8 Schematic of Thrust Balance

Figure 8 shows the working principle of the thrust balance schematically. When the thruster fires, the pendulum deflects and the optical measurement system detects the movement.

Figure 9 through 11 show the realization of this method. As seen in figure 9 the pendulum hangs from torsion springs inside the vacuum chamber. Since torsion springs were used the deflection can be assumed to be frictionless; this allows for easier calibration. The fixed part of the design is welded to the inner wall of the chamber. The pivot bearing is mounted in order to allow alignment around the z-axis as well as in the x-y-plane, see figure 10. The frame, to which the thruster is fixed is balanced out and screwed to the pendulum. The measurement unit is positioned at the very bottom of the structure in order to obtain maximum deflection values.

The deflection is measured by using an optical position encoder. In principle, this technology uses a readhead and a self adhesive scale. This scale is attached to the pendulum, while the readhead is positioned perpendicular to the direction of motion 0.7 mm away from the scale, see figure 11.

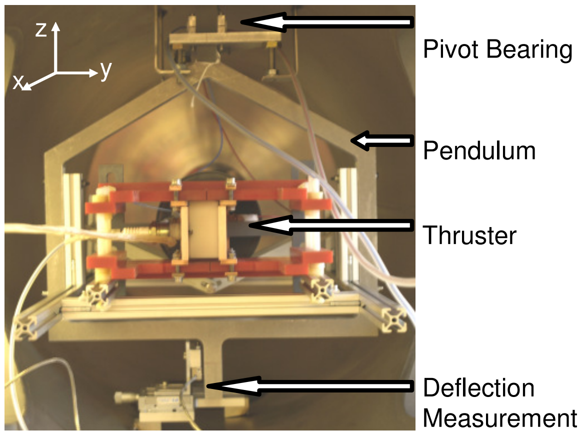

Fig. 9 Thrust Balance inside Vacuum Chamber

The readhead consists of a LED and a photodiode. The scale is a measuring tape -like device, its gold coated divisions enable the photodiode to detect a change in signal as the scale and the redhead move relative to each other. The readhead is mounted on a platform, which is welded to the vacuum chamber.

The thrust balance will be calibrated by using a piezo impulse hammer mounted on a stroke magnet.

Currently, all parts of the thrust balance have been manufactured and assembled inside the vacuum chamber and first data is awaited.

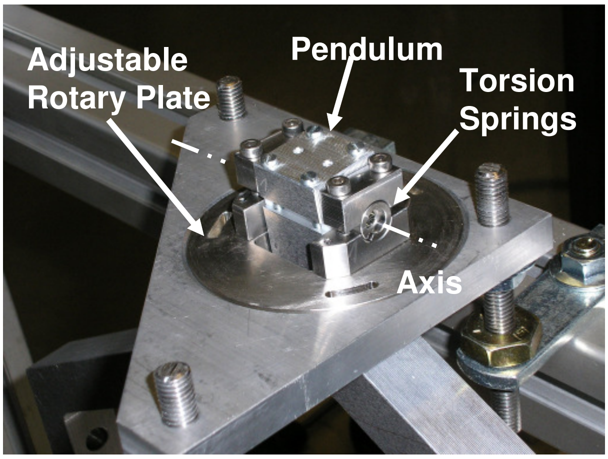

Fig. 10 Close-Up of Pivot Bearing

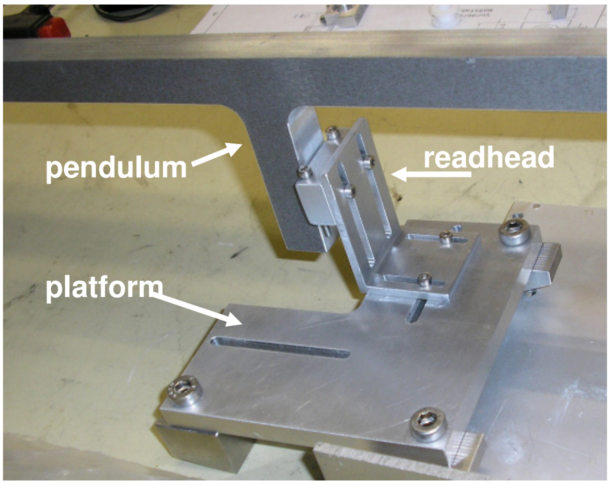

Fig.11 Close-Up of Deflection Measurement Unit

The Slug Model

It is possible to make a qualitative statement about important thruster parameters like specific impulse or thrust based on the current and mass measurements made. For this purpose the slug model [6] was used. For the thruster geometry used it is not possible to assume a constant magnetic field throughout the space between the electrodes, a more precise model was deduced.

In the following, a summary of the slug model implemented will be given. A more detailed explanation can be found in [7].

The two equations below describe the slug model. One of them describes the acceleration of the plasma by the acting Lorentz force. The other contains the information about charge distribution within the circuit according to Kichhoff law. For the second equation an equivalent circuit diagram as seen in figure 12 is used. A capacitor with the capacity C discharges over the circuit formed by the plasma and the electrodes. The changing resistance of the plasma is accounted for by the term R(t). The circuit has an initial inductance L_0 and a time dependent inductance L(t), caused by the moving plasma sheet.

Within this model, the plasma sheet is assumed to be perpendicular to the electrodes at all times and the current density is assumed to be constant within the sheet.

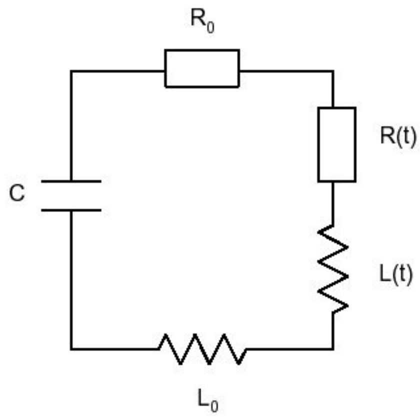

Fig. 12 RLC Circuit Assumed for Plasma Dynamics

The following two equations describe the slug model.

$$F = \int (\vec{j} \times \vec{B}) dV = m_{bit} \ddot{x} \qquad \text{Eq.1}$$

$$V_0 - \frac{1}{C} \int_0^T J dt = RJ + L_1 \dot{x} J + (L_0 + L_1 x) \dot{J} \qquad \text{Eq.2}$$

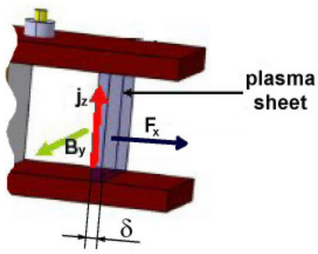

Fig.13 Schematic of Lorentz Force accelerating the Plasma Sheet

The Lorentz force equation 1 is the cross product between the current density j and the magnetic field B, integrated over the volume V of the plasma sheet. The mass bit m_{bit} ablated per pulse is accelerated along the direction x of the channel. In the second equation the initial voltage V_0 stored in the capacitor discharges through the plasma, creating a current J. The derivatives with respect to time are denoted as $\dot{x}, \ddot{x}, \dot{J}$. L_1 is the change in inductivity over the traveled distance x and is found to be [7,8]:

$$L_1 = \mu \frac{h}{d} K_{dh} \,. \qquad \text{Eq.3}$$

Here μ is the magnetic permeability and h and d are the distance between the electrodes and the width of the electrodes respectively. The factor K_{dh} takes the variation of the magnetic field for different quotients h/d into account. For the values of h/d (between 0,4 and 1) considered here, K_{dh} is about 0.6. Hence, if the calculations had been performed assuming a constant magnetic field, the error would have been ~40 %.

Assuming the plasma sheet as seen in figure 13, the two components causing the acceleration of the plasma are the magnetic field in y-direction and the current density in z-direction. From the Maxwell equation the magnetic field in y-direction can be derived:

$$B_y = \frac{\mu J}{2\pi d}\left(1 - \frac{x}{d}\right)(\vartheta_1 + \vartheta_2) \,. \qquad \text{Eq.4}$$

The geometric values ϑ_1, ϑ_2 and the factor K_{dh} both originate from the same physical circumstance of a varying magnetic field. With equation 4 and assuming constant current density inside the plasma equation 1 can be simplified:

$$F_x = \int \vec{j}_z \vec{B}_y dV = \frac{1}{2} L_1 J^2 = m\ddot{x}$$

Eq.5

This equations eq.2 and eq.5 were fed with data from the current measurement, the mass bit and constants and was solved for the distance x the plasma has traveled.

Results

Measurements of current over time as well as the mass bit were conducted for the above mentioned parameter variations. The length of the electrodes is equivalent to the distance the plasma travels within the channel and was kept at 80 mm during this first batch of tests. Once the optimal parameter combination between the height and the propellant type was chosen, the length of the electrodes was varied in a second batch. Lengths tested were 80 mm, 70 mm, 60 mm and 47 mm.

In order to decide between configurations the current measurements were fed into the slug model described above. It is possible to derive a qualitative result about characteristic values of the thruster. However, it is important to note that no conclusion about the quantity of any of values derived from the model can be drawn. The results from the model are purely qualitative. The results serve as criteria to determine the most suitable configuration for the proposed lunar mission. The propellant exhaust velocity, the impulse bit, i.e. the impulse created by one pulse and the electric efficiency of the thruster were investigated. The impulse bit directly corresponds to the mean thrust. The exhaust velocity is a direct solution of the equation system eq.1 and eq.2. The equations for impulse bit I_{bit} and electric efficiency η_{el} are given below.

$$I_{bit} = \frac{1}{2} L_1 \int_0^{t_f} J^2 dt \qquad \text{Eq.6}$$

$$\eta_{el} = \frac{\int_0^{t_f} \frac{1}{2} \dot{L} J^2 dt}{\int_0^{t_f} JV dt} \qquad \text{Eq.7}$$

The electric efficiency describes the fraction of the electric energy supplied to the capacitor (denominator) that is converted to energy used for acceleration of the plasma during the time t_f.

Figure 14 shows a typical graph of the oscillating current. Time divisions are 5 μs and one division in y direction equals 10 kA for the current. Within about 8 ms the current reaches a peak of up to 30 kA. A photodiode was used to show that every oscillation causes a new ablation. This behavior is well described in [6]. However, these oscillations diminish the efficiency of the thruster and are not wanted. The slug model applies only to the first half period. For the other periods the assumption of the ablated mass being the only mass accelerated does not hold true. The second ablation for instance encounters residual plasma from the first ablation, etc.

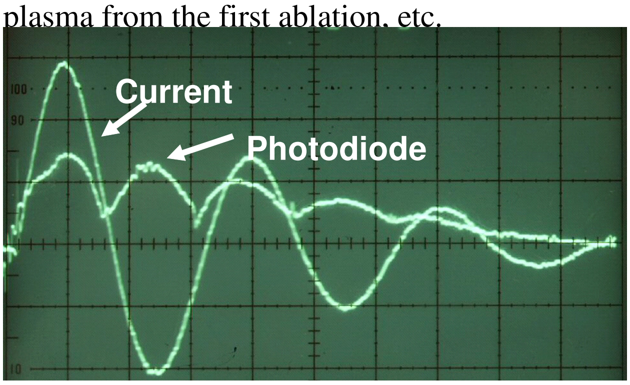

Fig.14 Oscilloscope Graph of Current and Photodi ode over Time [5μs/div]

Hence, only this first half period is investigated in the following. The mass bit calculated from the difference in propellant mass accounts for all ablations per pulse. A model connecting the energy within one ablation to the mass bit ablated was established [7]. However, since qualitative results remain the same this model will not be used here.

Figure 15 shows the experiments conducted with pure PTFE. As expected, an increase in distance between the electrodes reduces the current peak. Equivalent results were found for the propellant containing MoS_2. The metal did not cause any difference in behavior of the current.

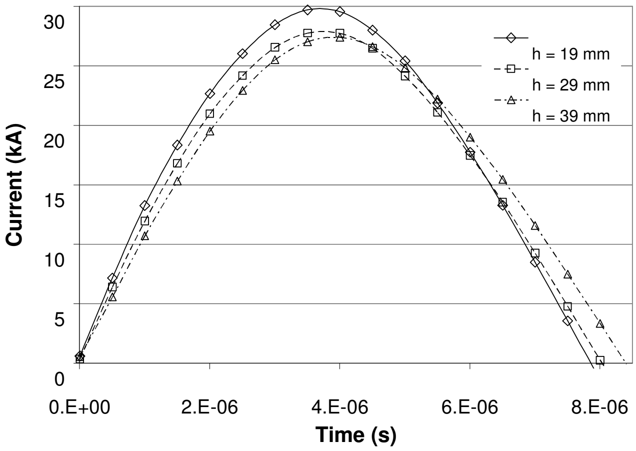

Fig.15 Half Period Current vs. Time for Three Different Distances Between Electrodes

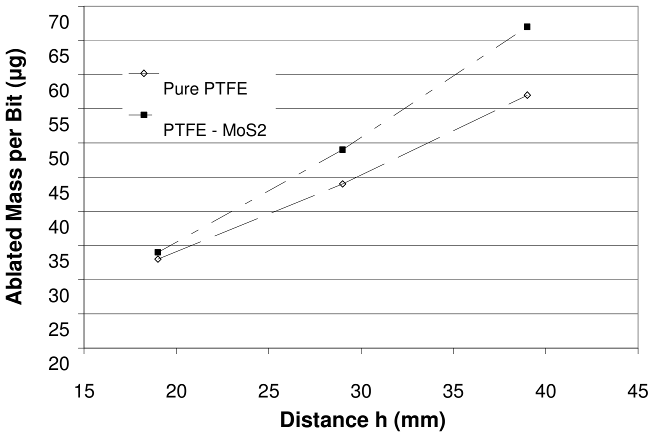

Fig.16 Ablated Mass Bit per Pulse

The ablated mass per pulse increases with the distance h between the electrodes, as seen in figure 16. This is explicable, since the ablation area increases. However, this means that even at a distance of 39 mm the initial energy density between the electrodes is sufficient to cause ablation.

From these values for current and mass bit the exhaust velocity, the impulse bit and the efficiency were derived qualitatively by solving the slug model and using equations 6 and 7.

The exhaust velocity reduces with increase in h, figure 17. This is due to the fact that less energy per mass is available for acceleration. However, the other parameters, the impulse bit as well as the efficiency increase with h, as seen in figures 18 and 19.

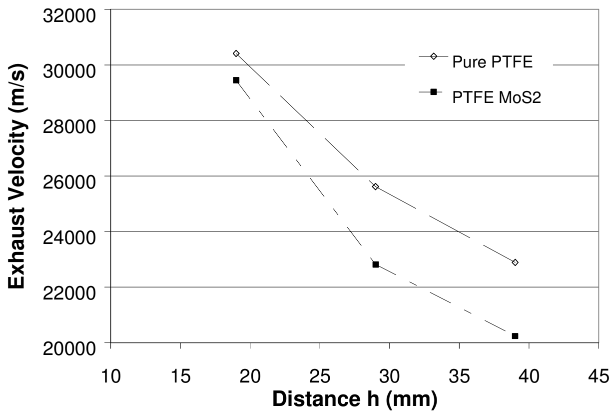

Fig. 17 Exhaust Velocity Decreases with Increasing Distance between Electrodes

In order to explain this, a closer look needs to be taken at the derivation of these quantities. Two parameters influence the impulse bit: L_1 and $\int J^2$. These two parameters affect I_{bit} in opposite ways. While L_1 increases with the distance h, the integral $\int J^2$ reduces.

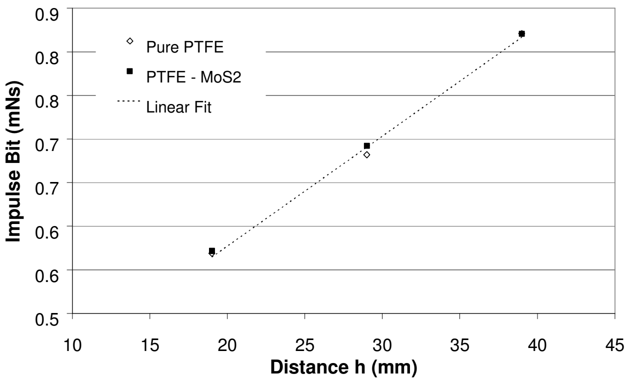

Fig.18 Impulse Bit per Pulse for two Types of PTFE

This results in an almost linear increase of the impulse bit, figure 18. Regarding the impulse there is no significant difference between the two propellants investigated.

The main parameters influencing the efficiency shown in figure 19 are the two ratios $\frac{\dot{L}}{R}$ and $\frac{\Delta L}{L_0}$ [6]. The resistance R is the mean resistance over the first half period calculated from the current data obtained [6,9]. $\dot{L}$ is the change in inductivity with respect to time and can be written as:

$$\dot{L} = L_1 \dot{x} \qquad \text{Eq. 8}$$

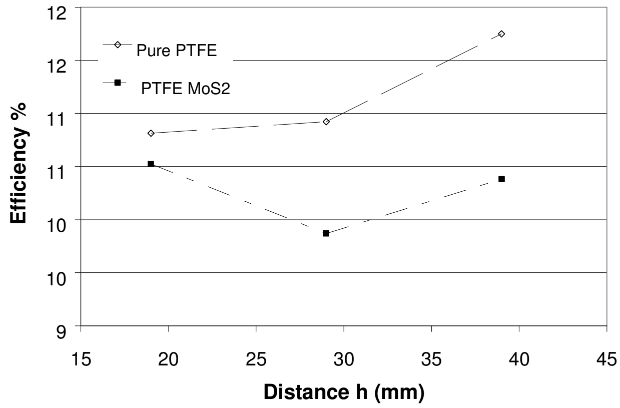

Fig. 19 Electric Efficiency over Distance between Electrodes

ΔL is the change in inductivity due to the plasma position. This means it is L_0 at the beginning of the discharge and Lend at the point x_f along the channel where the plasma is no longer accelerated, which is the end of the first half period.

$$\Delta L = L_{end} - L_0 = L_1 x_f \qquad \text{Eq. 9}$$

Both parameters $\frac{\dot{L}}{R}$ and $\frac{\Delta L}{L_0}$ increase with the distance h [7]. Further analysis of these ratios shows that the only factor increasing with h is the inductance per unit length L_1. In fact, both denominators R and L_0 increase. Nevertheless, the increase in L_1 is sufficient to let ΔL and $\dot{L}$ follow.

Both the exhaust velocity and the efficiency show that using pure PTFE is clearly favorable over PTFE to which MoS_2 was added. The increase in efficiency that was hoped for when using the PTFE alternative could not be confirmed.

As to the distance h between the electrodes the configuration with the highest exhaust velocity was chosen. This is due to two facts. One, a high exhaust velocity plays a crucial role on the lunar mission because of better payload to structure mass ratios. Secondly, it could be shown that the impulse bit as well as the efficiency increase because of L_1 only. L_1 on the other hand increases because of higher h/d values inherent to the configurations with larger h. This means, there are other possibilities to increase L_1, even when the distance h is kept low. For instance, the width d of the electrodes could be reduced. This means that optimally the same high exhaust velocity can be maintained while the efficiency and the impulse bit are increased.

In a second batch of tests, a distance h of 19 mm and pure PTFE were used. The length of the electrodes was gradually decreased in order to optimize current oscillation behavior. It was hoped to reduce the number of oscillations seen in figure 14. However, varying the length from 80 mm to 47 mm did not lead to any significant change in results.

Outlook

The next steps on the facility side include the completion of the life expectancy test stand as well as first measurements with the thrust balance. Measurements from the thrust balance can then be used to crosscheck the results obtained from current measurements in combination with the slug model. Further measurement techniques planned include a charged coupled device (CCD) camera, which will be used to investigate the movement of the plasma sheet at different times during the acceleration. On the thruster side, it is important to optimize current oscillation behavior. Amongst other measures this will include reducing the width of the electrodes, exploring different capacitor types and investigating further reduction of electrode length.

Acknoledgements

The authors thank the *Deutsches Zentrum für Luft und Raumfahrt (DLR)* for their funding of this project under contract number FKZ-50-JR-0446.

References

1. G. Grillmayer, M. Lengowski, S. Walz, H.-P. Röser, F. Huber, M. v. Schönermark, T. Wegmann: *Flying Laptop - Micro-Satellite of the University of Stuttgart for Earth Observation and Technology Demonstration*. IAC-04-IAA.4.11.P.08, 55th IAC, Vancouver, Canada, October 4-8, 2004.
2. M.H. Graesslin, H.-P. Roeser, *Cermit: Controlled Earth Reentry Mini-Vehicle to Improve Technology*, IAC-04-V.6.09, 55th IAC, Vancouver, 2004
3. R. Laufer, M. Auweter-Kurz, M. Lengowski, A. Nawaz, H.-P. Roeser, M. v. Schoenermark, H. Wagner *An All Electrical Small Satellite for a Technology Demonstration and Science Mission to the Moon.* IAC-04-Q.2b.05, 55th IAC, Vancouver, 2004
4. M. Riehle, H.L.Kurtz, M. Auweter-Kurtz *Hydrazine Arcjet System Development*. 25th IEPC, 1997 Cleveland, Ohio
5. A. Nawaz, M. Auweter-Kurtz, H. Kurtz, H.P. Wagner *Pulsed Plasma Thrusters for Primary Propulsion and Attitude Control of a Small All Electrical Satellite*. International Space Propulsion Conference, Sardinia, Italy, 2004.
6. R.G. Jahn *Physics of Electric Propulsion.* McGraw-Hill Series in Missile And space Technology, McGraw-Hill 1968.
7. S. Palumberi *Initial Start-Up and Investigation of a Modular Ablative Pulsed Magnetoplasmadynamic Thruster*. Diplomarbeit, IRS-05-S-15 April 2005.
8. H.Knoepfel *Pulsed High Magnetic Fields* North Holland Publishing company, 1970.
9. C.A. Scharleman, T.M. York, P.J. Turchi *Investigation of a PPT Utilizing Water as a Component Propellant*. International Electric Propulsion Conference, 2003.